


# Solid Particle Effects in Centi-scale Slurry Bubble Columns

Adam Mühlbauer, Olivia Böck, Raphael Raab, Mark W. Hlawitschka, and Hans-Jörg Bart\*

DOI: 10.1002/cite.202000136

 This is an open access article under the terms of the Creative Commons Attribution License, which permits use, distribution and reproduction in any medium, provided the original work is properly cited.

**Dedicated to Prof. Dr.-Ing. Matthias Kraume on the occasion of his 65th birthday**

Both solid particles and column diameter affect the gas holdup and flow regimes in slurry bubble columns, but investigations of the combined effects are not to be found. This study shows the simultaneous impacts on the overall gas holdup and flow regime transitions and determines the dominant effects in slurry bubble columns on the centi-scale containing solid particle concentrations up to 20 vol %. Additional tomography measurements are presented to visualize the gas phase flow and the spatial gas phase distribution in the column.

**Keywords:** Electrical resistance tomography, Flow regime transitions, Slurry bubble columns, Solid particle effects, Wall effects

Received: July 10, 2020; revised: August 20, 2020; accepted: October 19, 2020

## 1 Introduction

Slurry bubble columns (SBCs) are widely applied as apparatuses in chemical industry, typically to carry out heterogeneously catalyzed reactions [1,2]. The fluidized solid particles heavily affect the fluid dynamics in the bubble columns (BCs) [3–5]. Recent investigations still tackle experimental [6,7] and numerical [8,9] approaches to characterize the gas phase dynamics in SBCs because of the solid particles influencing the coalescence and breakage behavior of bubbles. In addition, internals with other hydraulic diameters – corresponding to the ratio of the wetted perimeter and the flow cross-sectional area – than the column diameter have an impact on the fluid dynamics in BCs [10], e.g., bubble columns equipped with tube bundles [11]. Simultaneously, bubbles rising inside tube bundles can be imagined as a numbering-up of small (usually centiscale) BCs where wall effects play an important role.

The well-known flow regime map for water and dilute aqueous solutions is depicted in Fig. 1 where the wall effects on the flow regimes become already visible. The regime transitions depend mainly on the superficial gas velocity  $U_g$ . At low superficial gas velocities, bubbly flow emerges in which no bubbles coalesce. Besides, small column diameters  $D_c$  may stabilize bubble plugs at increased superficial gas velocities whereas the heterogeneous churn-turbulent flow occurs in wider columns.

Despite the fact that slurry bubble columns are widely spread in chemical industry, the regime map lacks solid particle effects. Previous investigations indicate effects of solid particles in SBCs on the flow regime transitions where the

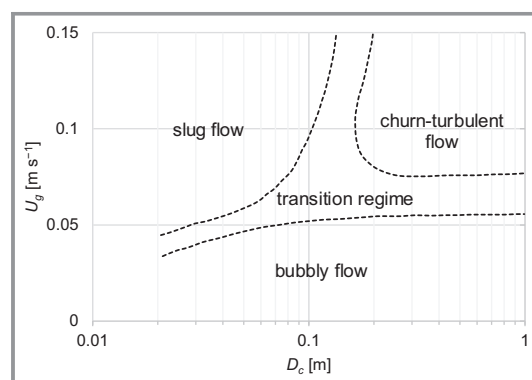


Figure 1. Flow regime map adopted from [2].

addition of small solid particles shifts the transition velocities to lower superficial gas velocities [12]. The addition of microparticles in SBCs changes the density and viscosity of the slurry and enhances coalescence of bubbles and results in lower gas holdups [3,4]. By contrast, heavy particles in the millimeter range may lead to breakage of bubbles and increase the gas holdup [13,14]. It was also observed that solid particles affect the bubble rise velocities where the

Adam Mühlbauer, Olivia Böck, Raphael Raab,  
 Dr.-Ing. habil. Mark W. Hlawitschka,  
 Prof. Dr. techn. Hans-Jörg Bart  
 bart@mv.uni-kl.de  
 Technische Universität Kaiserslautern, Lehrstuhl für Thermische  
 Verfahrenstechnik, Gottlieb-Daimler-Straße 44, 67663 Kaiserslautern,  
 Germany.

addition of microparticles reduces bubble velocities [4]. Further detailed investigations found that small particles can accumulate in the wakes of the bubbles and increase the net mass which results in lower bubble relative velocities [15, 16].

The present work studies the effects of solid particles and column diameter  $D_c$  on the gas phase dynamics and flow regime transitions in four SBCs on the centi-scale ( $D_c = 1.6, 3.2, 4.4, 10$  cm) where the transition from the bubbly to the slug flow occurs. An additional section covers the visualization of the two- and three-phase flows with tomographic methods.

## 2 Experimental

### 2.1 Column Setups

Cylindrical columns with various inner diameters are investigated to show the solid particle effects on the bubbly flow. Four similar experimental setups according to Fig. 2 are used. All columns were equipped with perforated-plate (PP) gas distributors where the holes were equally distributed all over the column cross section. The detailed characteristics of the setups can be found in Tab. 1.

The aspect ratios

$$A_0 = \frac{H_0}{D_c} \quad (1)$$

with the liquid filling height  $H_0$  and the column inner diameter  $D_c$  vary between 9 and 25. For large industrial columns with  $H_0 > 1-3$  m, the gas holdup is independent of the filling height if  $A_0 > 5$  [17]. However, wall effects may occur in small bubble columns with  $D_c \leq 10$  cm [18].

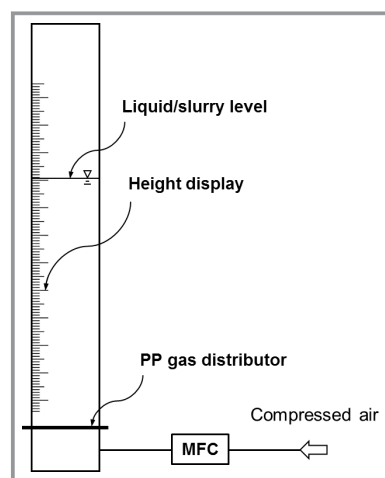


**Figure 2.** General schematic of the experimental setups.

**Table 1.** Characteristics of the investigated BCs.

BC No.	1	2	3	4
Inner diameter $D_c$ [cm]	1.6	3.2	4.4	10
Height $H_c$ [m]	1.0	1.0	1.0	2.0
Liquid/slurry filling height $H_0$ [m]	0.400	0.400	0.400	1.20
Aspect ratio $A_0$ [-]	25.0	12.5	9.09	12.0
PP hole diameter $D_h$ [mm]	0.5	0.5	0.5	0.4
PP hole pitch $P_h$ [mm]	2.8 (square)	2.8 (square)	2.8 (square)	7.0 (triangular)
Number of holes $N_h$ [-]	21	89	177	163
Open area $A_h$ [-]	$2.1 \times 10^{-2}$	$2.2 \times 10^{-2}$	$2.3 \times 10^{-2}$	$0.26 \times 10^{-2}$

The PP hole diameters  $D_h$  were chosen to be similar because they may have an effect on the total gas holdup (smaller  $D_h$  results in higher gas holdup) [19]. Though, the open areas

$$A_h = \frac{N_h D_h^2}{D_c^2} \quad (2)$$

differ and are around 2% of the cross-sectional area for the small columns ( $D_c = 1.6, 3.2, 4.4$  cm) and are significantly smaller than 1% for the largest column ( $D_c = 10$  cm). It has been found that the gas distributor design may delay the onset of regime transitions [20] and very recent studies show that PP gas distributors with open areas  $A_h > 1\%$  shift the first transition velocity to a higher superficial gas velocity [21]. Due to keeping the ratios  $A_0$  and  $A_h$  constant for all measurement series in the different columns, it is still possible to evaluate the effects of solid particles on the gas holdup and the flow regime transitions.

The superficial gas velocities  $U_g$  were adjusted with a mass flow controller (MFC) from Brooks Instrument® (GF040 series).  $U_g$  was increased in steps of  $\Delta U_g = 1 \text{ cm s}^{-1}$  in the small columns ( $D_c = 1.6, 3.2, 4.4$  cm) and of  $0.5 \text{ cm s}^{-1}$  in the large column ( $D_c = 10$  cm), respectively. Air from a compressed air supply was used to aerate the column and desalinated water was used for the liquid in BCs with  $D_c = 1.6, 3.2, 4.4$  cm and tap water in BC with  $D_c = 10$  cm, respectively. All experiments were repeated with spherical soda-lime glass particles ( $\rho_s = 2500 \text{ kg m}^{-3}$ ,  $70 \mu\text{m } q_3$  mean,  $100 \mu\text{m}^2 q_3$  variance) in the liquid in concentrations of 10 and 20 vol%. All measurement series were carried out at room temperature (approx.  $20^\circ\text{C}$ ) and atmospheric pressure (approx. 1 bar).

## 2.2 Measurement and Evaluation Techniques

### 2.2.1 Gas Holdup Measurements

The gas holdups were evaluated statistically according to the following technique. Photographs were taken with a

Nikon D5600 reflex camera positioned horizontal to the column at the aerated liquid/slurry level for every operating point (i.e., every  $U_g$ ). The aerated levels were evaluated from the photos consistently at the same vertical line on the column inside wall.

Fig. 3 indicates the vertical dashed lines on the inner wall and the evaluated aerated continuous phase levels  $H_{cd}$ . The instantaneous level  $H_{cd}$  was read off where the surface of the liquid/slurry appeared on the dashed line in the image. For every  $U_g$ , 20 sequential photos were analyzed to evaluate the gas holdup according to

$$\varepsilon_g = \frac{H_{cd} - H_0}{H_{cd}} \quad (3)$$

The mean  $\bar{\varepsilon}_g$  and the standard deviation  $\sigma_\varepsilon$  of all evaluated instantaneous gas holdups were calculated as

$$\bar{\varepsilon}_g = \frac{1}{N} \sum_{i=1}^N \varepsilon_{g,i} \quad (4)$$

$$\sigma_\varepsilon = \sqrt{\frac{1}{N-1} \sum_{i=1}^N (\varepsilon_{g,i} - \bar{\varepsilon}_g)^2} \quad (5)$$

with the number of images per operation point  $N = 20$ .

### 2.2.2 Determination of Flow Regime Transitions

As indicated in Fig. 1, in the column diameter range up to 10 cm (i.e., centi-scale) the bubbly flow (homogeneous), the slug flow (heterogeneous) as well as a transition regime exist depending mainly on the superficial gas velocity. In this work, the authors determined the flow regime transitions of the gas-liquid/slurry flows in all investigated columns as well.

Fig. 4 shows the onset of the transition regime T1 and the onset of slug flow T2 when increasing  $U_g$  for 0 and 20 vol %

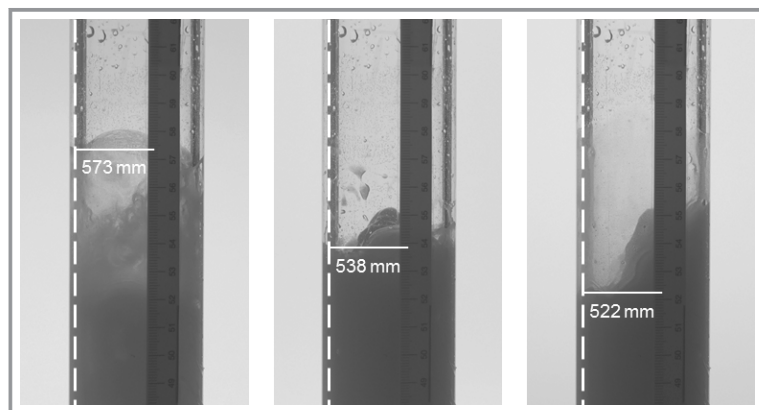


**Figure 3.** Illustration of the level evaluation of three sequential images ( $D_c = 4.4$  cm).

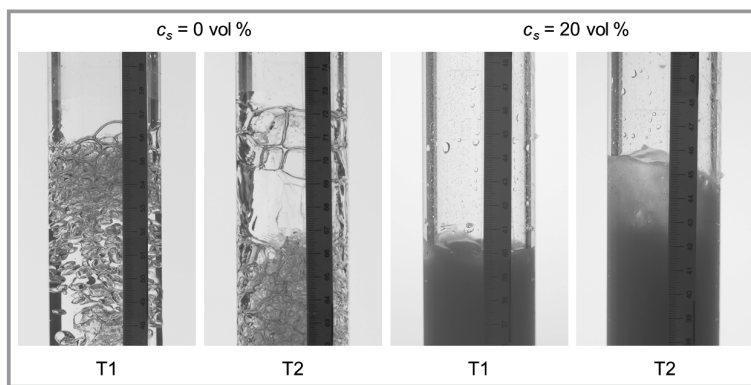


**Figure 4.** Exemplary illustration of the flow regime transition points T1 and T2 ( $D_c = 4.4$  cm).

solid concentration  $c_s$ , respectively. The criteria for the classification of the regimes are listed in Tab. 2.

The characteristics in two-phase flows are reported in [18, 22] and were adapted to three-phase flows, but the visual determination is more difficult in the opaque slurries. Therefore, the coalescence of bubbles at the slurry surface was observed carefully.

The transition points T1 and T2 could be determined by visual classification where the characteristics change according to Tab. 2. The maximum quantization deviation of the transition velocity  $\varepsilon_T$  depends on the superficial gas velocity step size of the measurement series according to

$$\varepsilon_T \leq \Delta U_g \quad (6)$$

This means that the transitions might occur close to the previous/following superficial gas velocity as well and is a measure of uncertainty of the determined transition velocities.

### 2.2.3 Electrical Resistance Tomography

The gas phase was visualized with electrical resistance tomography (ERT) in the largest column with  $D_c = 10$  cm. The flange type ERT sensor manufactured by Industrial Tomography Systems (ITS) is depicted in Fig. 5.

The sensor contains two measurement planes with a circular arrangement of 16 electrodes on each plane. The electrodes are in contact with the conductive liquid. The measurement procedure of the ERT system can be imagined by an excitation of one pair of electrodes while the voltage between another electrode pair is measured. The excitation and measurement sequences follow the adjacent strategy. Voltage is injected into a pair of neighboring electrodes with simultaneous measurement of the current. In addition, voltage is measured in the sub-sequential adjacent electrode pairs [23]. The procedure is repeated until all independent measurements

**Table 2.** Characteristics of the investigated flow regimes.

Regime	Solid concentration $c_s$	Characteristics
Bubbly	0	non-coalescent bubbly flow with monodisperse (perfect) or polydisperse (imperfect) bubble size distributions
	> 0	could not be observed
<i>Transition point T1</i>		
Transition	0	onset of coalescence (typically in core flow)
	> 0	irregular coalescence of very different sized bubbles at the slurry/ambient air interface
<i>Transition point T2</i>		
Slug	0	appearance of bubble plugs or Taylor bubbles
	> 0	regular coalescence of large bubbles at the slurry/ambient air interface and slurry level oscillations



**Figure 5.** Mounted ERT sensor ( $D_c = 10$  cm).

are taken. The measurements are realized with the data acquisition system v5r from ITS.

A cross-sectional image can be reconstructed from the independent measurements. The non-iterative reconstruction algorithm called modified sensitivity back-projection (MSBP) was used for the reconstruction of the conductivity tomograms [24]. Cross-sectional images of the local gas volume fraction  $\varepsilon_g$  are calculated from the conductivity tomograms with Maxwell's equation which reads for a non-conductive secondary phase [25] as

$$\varepsilon_g = \frac{2\sigma_c - 2\sigma_{cd}}{2\sigma_c + \sigma_{cd}} \quad (7)$$

A reference measurement has to be taken before aerating the column to calibrate the voltage signals with the separately measured conductivity of the continuous phase. A conductivity  $\sigma_{c,l} = 0.165 \text{ mS cm}^{-1}$  of the water and  $\sigma_{c,sl} = 0.190 \text{ mS cm}^{-1}$  of the slurry was measured with

the Seven2Go™ Pro Conductivity Meter S7 from Mettler Toledo.

For the investigated superficial gas velocities, 60 000 tomograms were recorded with a frequency of 312.5 Hz. The high temporal resolution is still one of the advantages of ERT and allowed the visualization of the different flow regimes in this study.

## 3 Results

### 3.1 Gas Holdup Measurements

The dependency of the solid particle concentration  $c_s$  and the column diameter  $D_c$  on the gas holdup is shown in Fig. 6.

The gas holdup profile is independent of  $c_s$  in the smallest column where the wall effect is dominant. In the middle-sized columns, the presence of solid particles can be recognized in the gas holdup profiles. However, the gas holdup profiles hardly differ with respect to different solid concentrations. In the largest column, even the concentration of solid particles (10 and 20 vol %) is noticeable in the gas holdup profiles where the holdup decreases with increasing  $c_s$ .

In the smallest column, the solid particle effect is negligible and becomes more important with increasing  $D_c$  over the centi-scale. The solid particles seem to have a significant effect on the flow regimes for columns with about  $D_c > 3$  cm. For  $D_c = 10$  cm, even a change in the concentration of solid particles becomes recognizable in the gas holdup profiles where the wall effect is weak.

Furthermore, there are similar holdup profile characteristics of the pure wall effect ( $D_c = 1.6$  cm and  $c_s = 0$  vol %) and the dominant solid particle effect ( $D_c = 10$  cm and  $c_s = 20$  vol %). The gas holdup is increasing slowly with  $U_g$  and a pronounced curvature of the profile is missing. This is due to the stabilization of large bubbles in small columns

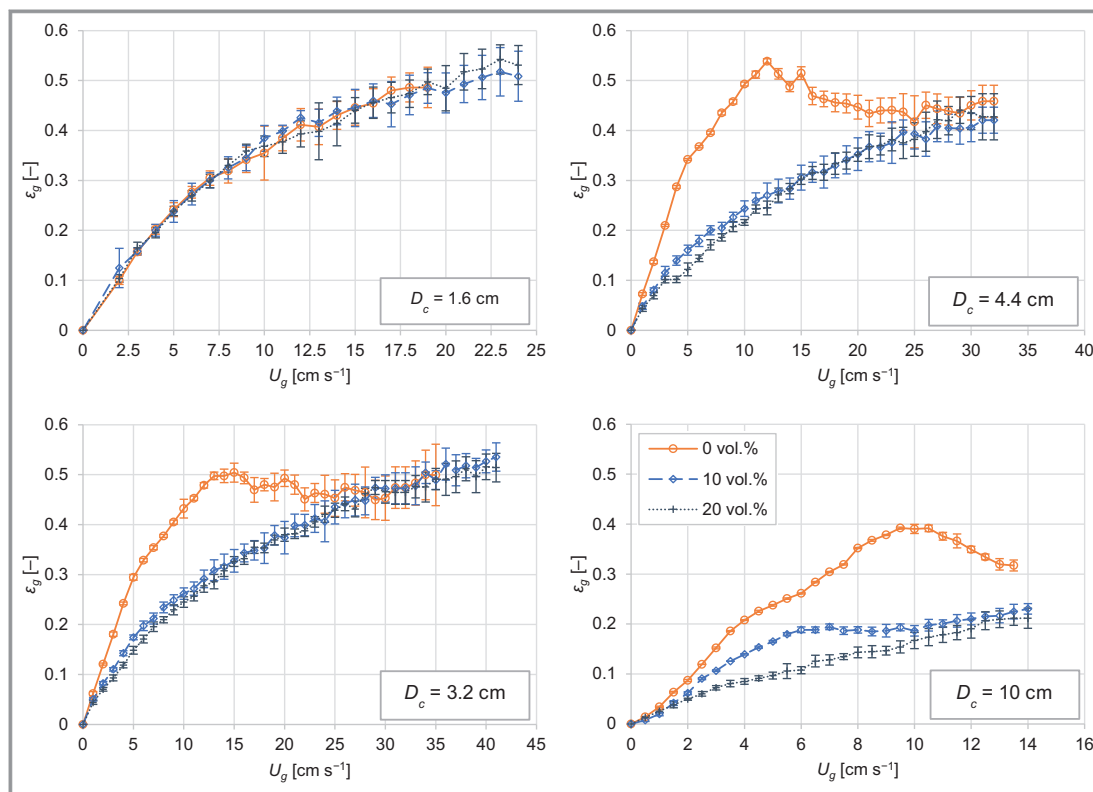


**Figure 6.** Gas holdup in four different sized BCs dependent on solid concentration (legend in last diagram valid in all diagrams).

(independent of  $c_s$ ) as well as in larger columns at high solid concentrations.

The presence of large bubbles can be deduced from the aerated level oscillations. The oscillations occur in two- and three-phase flows in the small columns and can be still found at the highest measured solid concentration in the largest column. The fluctuations are visualized in Fig. 6 with error bars  $\pm\sigma_\epsilon$  indicating the standard deviation of all evaluated instantaneous gas holdups according to Eqs. (3)–(5) per operating point (max. 0.06 for slug flow). The pronounced level oscillations indicate slug flow in the column and can be additionally taken as a hint for the transition point T2.

Another noticeable characteristic is the converging slug gas holdup profiles at high gas throughputs in centi-scale BCs. At high gas throughputs, the wall effect becomes dominant again independent of the solid particle concentration, which could be observed in the three small columns ( $D_c = 1.6, 3.2, 4.4 \text{ cm}$ ). In the largest column ( $D_c = 10 \text{ cm}$ ), the superficial gas velocities could not be adjusted high enough to confirm this phenomenon. However, the solid particle effect plays an important role because the convergence of the profiles occurs more rapidly in the presence of solid particles where coalescence of bubbles is enhanced and large bubbles get stabilized more easily. Therefore, the solid particle effect also affects the flow regime transitions in SBCs.

### 3.2 Regime Transition Velocities

The observed flow regime transitions are depicted in Fig. 7. The transition points were chosen to be the superficial gas velocities  $U_g$  where the regime criteria changed according to Tab. 2 and were assigned with the quantization deviation  $\pm\epsilon_T$ . Only for the largest column, the observed transitions agree with the indicated literature values of [2]. Various gas distributor designs may account for the differences as is already mentioned by [2]. The observed transition velocities are not monotonically increasing with  $D_c$  as expected from the literature trend which might arise due to different open areas of the gas distributors as well. The large open areas of the gas distributors in the three small columns may lead to a gas maldistribution and different offsets in the regime transitions. However, the trends of the transition points change to monotonically increasing profiles as  $c_s$  increases. Presumably, the gas sparger design and gas maldistribution do not play such an important role in coalescent dispersed gas phase systems as long as the inlet bubble diameter is smaller than the stable bubble diameter in the BC.

The important main trend that emerges from the observations is the shift of the transition points T1 and T2 towards smaller  $U_g$  in the presence of solids. Bubbly flow could not be observed at all and once solid particles are present, the transition regime is immediately reached with the onset of coalescence. As a consequence, the curves of T1



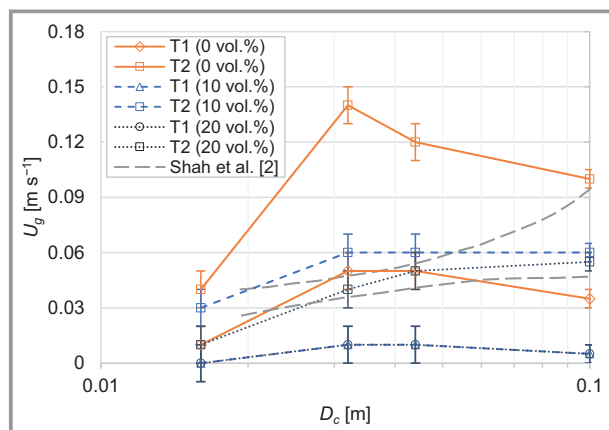


**Figure 7.** Regime transition map for the investigated BCs and SBCs.

coincide for different solid concentrations. T2 is also lowered in the presence of solid particles, even if only a weak dependency can be found. Thus, an increase in  $c_s$  is accompanied by a regime transition point T2 at lower superficial gas velocities.

### 3.3 Flow Regime Visualizations

All observed flow regimes were additionally investigated by using ERT in the largest column with an inner diameter  $D_c = 10$  cm. In the top row of Fig. 8, the visualizations of the flow regimes are shown for  $c_s = 0$  and 10 vol.%. The horizontal axis in the ERT images represents the column width and the vertical axis represents the time domain where every image shows 0.8 s of measurement time. Thus, the images show gas volume fractions (light areas) passing the tomography plane at  $z = 75$  cm. The dark gray areas depict the continuous phase (liquid or slurry).

The regime transition offset induced by solid particles becomes clearly visible in the flow visualizations. For  $U_g = 2$  cm s<sup>-1</sup>, the two-phase flow is still in the bubbly regime whereas the three-phase flow is already transitioning, and for  $U_g = 8$  cm s<sup>-1</sup>, the transition regime can be observed for 0 vol.% and the slugging regime for 10 vol.% particle concentration.

In the bottom row of Fig. 8, the time-averaged local gas volume fraction profiles  $\varepsilon_g$  along the radial position  $r$  in the column are shown. The

same trends can be seen as already indicated in Fig. 6 and additionally the radial resolution of the gas-phase volume fraction becomes visible. Bubbly flow is recognized with a very flat gas volume fraction profile across the column width. The profiles show stronger gradients in the transition and even more in the slugging regime.

Thus, solid particle effects on the spatial gas fraction distributions can be shown with ERT and may also serve for comparison with 3D simulations, e.g., computational fluid dynamic (CFD) simulations. Furthermore, such a data base is still necessary with regard to model development and testing for disperse gas-liquid-solid flows, especially including breakage and coalescence phenomena [26].

## 4 Summary

Four different sized columns were investigated to show the effects of column diameter and solid particle concentration on the gas holdup and flow regime transitions. The main results of the study are:

- The wall effect is independent of the solid concentration in the smallest column with  $D_c = 1.6$  cm.
- For larger diameters  $D_c = 3.2, 4.4$  cm, the solid particle effect becomes more dominant and the solid concentration becomes even decisive in large columns with  $D_c \geq 10$  cm.

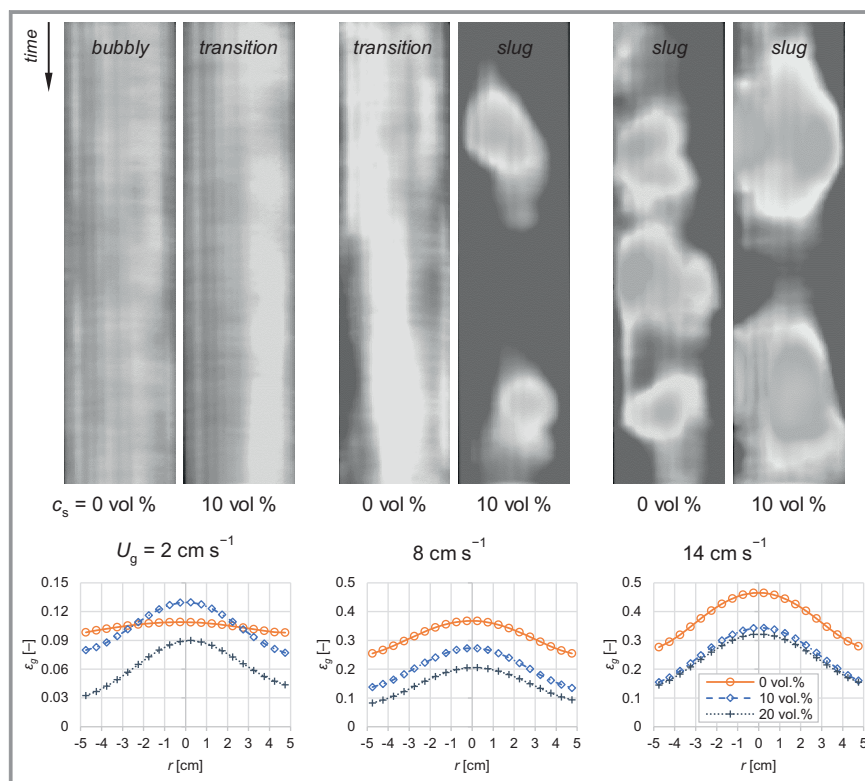


**Figure 8.** ERT measurements at  $z = 75$  cm (legend in last diagram valid in all diagrams).

- At high superficial gas velocities  $U_g$  when slug flow fully emerged, the wall effect is dominant independent of the solid particle concentration  $c_s$  and could be shown for  $D_c = 1.6, 3.2, 4.4$  cm.
- The presence of solid particles lowers both transition points T1 (bubbly-to-transition) and T2 (transition-to-slug) towards lower superficial gas velocities with increasing solid concentration. Pure bubbly flow completely vanishes.
- ERT is able to depict the solid particle effects on the gas phase dynamics and to characterize the gas phase spatial distributions in both BCs and SBCs.

Further studies address the data acquisition with ERT in SBCs to create a database, which is also appropriate for comparison with simulation data to support the development and validation of models suitable for CFD simulations. The studies can be extended to cover the effects of different particle properties (density, diameter, shape, etc.) on the gas volume fraction distribution and the large bubble velocities to characterize the coalescence behavior of bubbles in various slurries.

The authors gratefully acknowledge the support given by the Deutsche Forschungsgemeinschaft (DFG) funded Research Training Group RTG 1932 “Stochastic Models for Innovations in the Engineering Sciences”. Open access funding enabled and organized by Projekt DEAL.

### Symbols used

$A_0$	[-]	aspect ratio
$A_h$	[-]	open area
$c_s$	[vol %]	solid particle concentration
$D_c$	[m]	column inner diameter
$H_0$	[m]	column filling height
$H_c$	[m]	column height
$H_{cd}$	[m]	aerated liquid/slurry level
$N$	[-]	number of images
$N_h$	[-]	number of holes
$P_h$	[m]	pitch of holes
$q_3$	[m <sup>-1</sup> ]	particle volume density distribution function
$r$	[m]	radial coordinate in column
$U_g$	[m s <sup>-1</sup> ]	superficial gas velocity
$z$	[m]	dimension of column height

### Greek letters

$\varepsilon_g$	[-]	gas volume fraction
$\bar{\varepsilon}_g$	[-]	mean of gas volume fraction
$\varepsilon_T$	[m s <sup>-1</sup> ]	quantization deviation of transition velocity
$\rho_s$	[kg m <sup>-3</sup> ]	solid particle mass density

$\sigma$	[mS cm <sup>-1</sup> ]	conductivity
$\sigma_e$	[-]	standard deviation of gas volume fraction

### Sub- and superscripts

c	continuous phase
cd	mixture (continuous + disperse)
l	liquid
sl	slurry

### Abbreviations

BC	bubble column
CFD	computational fluid dynamics
ERT	electrical resistance tomography
MFC	mass flow controller
MSBP	modified sensitivity back-projection
PP	perforated-plate
SBC	slurry bubble column
T1	transition point bubbly-to-transition
T2	transition point transition-to-slug

### References

- [1] W.-D. Deckwer, A. Schumpe, *Chem. Ing. Tech.* **1985**, *57* (9), 754–767. DOI: <https://doi.org/10.1002/cite.330570909>
- [2] Y. T. Shah, B. G. Kelkar, S. P. Godbole, W.-D. Deckwer, *AIChE J.* **1982**, *28* (3), 353–379. DOI: <https://doi.org/10.1002/aic.690280302>
- [3] R. Krishna, J. W. A. de Swart, J. Ellenberger, G. B. Martina, C. Maretti, *AIChE J.* **1997**, *43* (2), 311–316. DOI: <https://doi.org/10.1002/aic.690430204>
- [4] H. Li, A. Prakash, *Powder Technol.* **2000**, *113* (1–2), 158–167. DOI: [https://doi.org/10.1016/S0032-5910\(00\)00228-X](https://doi.org/10.1016/S0032-5910(00)00228-X)
- [5] X. Luo, D. J. Lee, R. Lau, G. Yang, L.-S. Fan, *AIChE J.* **1999**, *45* (4), 665–680. DOI: <https://doi.org/10.1002/aic.690450402>
- [6] P. Tyagi, V. V. Buwa, *Chem. Eng. Sci.* **2017**, *173*, 346–362. DOI: <https://doi.org/10.1016/j.ces.2017.07.042>
- [7] J. N. Sines, S. Hwang, Q. M. Marashdeh, A. Tong, D. Wang, P. He, B. J. Straiton, C. E. Zuccarelli, L.-S. Fan, *Powder Technol.* **2019**, *355*, 474–480. DOI: <https://doi.org/10.1016/j.powtec.2019.07.077>
- [8] M. An, X. Guan, N. Yang, *Chem. Eng. Sci.* **2020**, *223*, 115743. DOI: <https://doi.org/10.1016/j.ces.2020.115743>
- [9] A. Mühlbauer, M. W. Hlawitschka, H.-J. Bart, *Exp. Comput. Multiphase Flow*, in press. DOI: <https://doi.org/10.1007/s42757-020-0078-y>
- [10] G. Besagni, F. Inzoli, *Chem. Eng. Sci.* **2016**, *145*, 162–180. DOI: <https://doi.org/10.1016/j.ces.2016.02.019>
- [11] S. S. Al-Shahrani, S. A. Nosier, A. H. El-Shazly, M. H. Abdel-Aziz, *Int. Commun. Heat Mass Transfer* **2020**, *113*, 104548. DOI: <https://doi.org/10.1016/j.icheatmasstransfer.2020.104548>
- [12] S. Rabha, M. Schubert, U. Hampel, *AIChE J.* **2014**, *60* (8), 3079–3090. DOI: <https://doi.org/10.1002/aic.14528>
- [13] Y.-M. Chen, L.-S. Fan, *Chem. Eng. Sci.* **1989**, *44* (1), 117–132. DOI: [https://doi.org/10.1016/0009-2509\(89\)85238-8](https://doi.org/10.1016/0009-2509(89)85238-8)
- [14] L.-S. Fan, O. Hemminger, Z. Yu, F. Wang, *Ind. Eng. Chem. Res.* **2007**, *46* (12), 4341–4346. DOI: <https://doi.org/10.1021/ie061532c>

- [15] M. Schlüter, S. Scheid, S. John, N. Rübiger, *J. Chem. Eng. Jpn.* **2004**, *37* (8), 947–954. DOI: <https://doi.org/10.1252/jcej.37.947>
- [16] M. Schlüter, S. Scheid, S. John, N. Rübiger, *Powder Technol.* **2005**, *151* (1–3), 68–76. DOI: <https://doi.org/10.1016/j.powtec.2004.11.032>
- [17] G. Besagni, F. Inzoli, *Chem. Eng. Sci.* **2017**, *170*, 270–296. DOI: <https://doi.org/10.1016/j.ces.2017.03.043>
- [18] N. Kantarci, F. Borak, K. O. Ulgen, *Process Biochem.* **2005**, *40* (7), 2263–2283. DOI: <https://doi.org/10.1016/j.procbio.2004.10.004>
- [19] J. Zahradník, M. Fialová, M. Růžička, J. Drahoš, F. Kaštánek, N. H. Thomas, *Chem. Eng. Sci.* **1997**, *52* (21–22), 3811–3826. DOI: [https://doi.org/10.1016/S0009-2509\(97\)00226-1](https://doi.org/10.1016/S0009-2509(97)00226-1)
- [20] R. C. Chen, J. Reese, L.-S. Fan, *AIChE J.* **1994**, *40* (7), 1093–1104. DOI: <https://doi.org/10.1002/aic.690400702>
- [21] S. Nedeltchev, F. Mörs, A. Mühlbauer, M. W. Hlawitschka, F. Graf, T. Kolb, H.-J. Bart, *Chem. Eng. Res. Des.* in press. DOI: <https://doi.org/10.1016/j.cherd.2020.11.013>
- [22] C. Leonard, J.-H. Ferrasse, O. Boutin, S. Lefevre, A. Viand, *Chem. Eng. Res. Des.* **2015**, *100*, 391–421. DOI: <https://doi.org/10.1016/j.cherd.2015.05.013>
- [23] F. Dickin, M. Wang, *Meas. Sci. Technol.* **1996**, *7* (3), 247–260. DOI: <https://doi.org/10.1088/0957-0233/7/3/005>
- [24] M. Wang, *Meas. Sci. Technol.* **2002**, *13* (1), 101–117. DOI: <https://doi.org/10.1088/0957-0233/13/1/314>
- [25] H. Li, M. Wang, Y.-X. Wu, G. Lucas, *Multiphase Sci. Technol.* **2009**, *21* (1–2), 81–93. DOI: <https://doi.org/10.1615/MultScienTechn.v21.i1-2.70>
- [26] A. Mühlbauer, M. W. Hlawitschka, H.-J. Bart, *Chem. Ing. Tech.* **2019**, *91* (12), 1747–1765. DOI: <https://doi.org/10.1002/cite.201900109>